1. Materials

The kinematic viscosity of each fluid was measured at 40°C and 100°C using a Houillon Viscometer and the densities were obtained using the ASTM D4052 method (1). The resulting calculated dynamic viscosity at both 40°C and 100°C of each blend are shown in **Table S1**.

#	Sample Label	$\eta_{40°C}$ (cP)	$\eta_{100°C}$ (cP)
1	99 wt% PIB + 1 wt% ZDDP	906	46
2	89 wt% PIB + 10 wt% PAO + 1 wt% ZDDP	802	43
3	84 wt% PIB + 15 wt% PAO + 1 wt% ZDDP	734	41
4	79 wt% PIB + 20 wt% PAO + 1 wt% ZDDP	675	40
5	74 wt% PIB + 25 wt% PAO + 1 wt% ZDDP	623	39
6	69 wt% PIB + 30 wt% PAO + 1 wt% ZDDP	580	38
7	64 wt% PIB + 35 wt% PAO + 1 wt% ZDDP	550	37
8	59 wt% PIB + 40 wt% PAO + 1 wt% ZDDP	512	36
9	54 wt% PIB + 45 wt% PAO + 1 wt% ZDDP	482	35

Table S1. Summary of estimated dynamic viscosity of each blend at 40°C and 100°C

2. Test methods

2.1   MTM experiment

The PCS Instruments MTM-SLIM™ (London, UK) generates both traction data and *in-situ* tribofilm thickness measurements (***Figure S1***)*.* Each test used 15 mL of lubricant in the MTM reservoir. The ball was loaded against the disk under a preset load for a fixed duration, and both were driven independently allowing different combinations of rolling and sliding speeds. The rotations were stopped at predetermined time intervals, whereupon the ball was loaded against the spacer layer-coated window. The SLIM camera then measured the tribofilm thickness, storing an interference image for post-processing. The measurement location on the ball was the same throughout the test. The SLIM methodology is described elsewhere (2). We also measured the final end-of-test film profile using aTencor™ P-7 (Milpitas, CA) 2-D surface profilometer to verify the accuracy of the SLIM measurements.
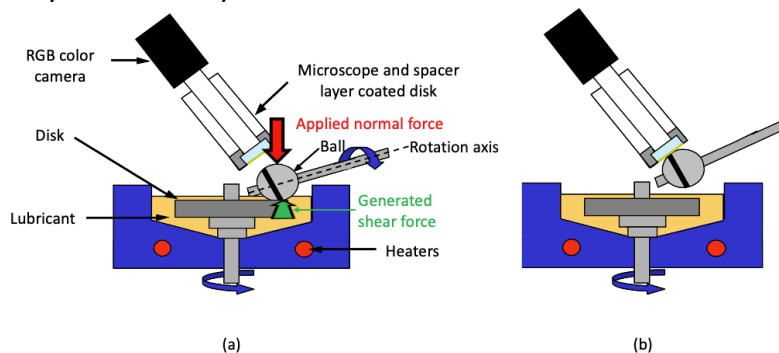

Figure S1. Schematic diagram of the MTM-SLIM setup (adapted from PCS Instruments' MTM-SLIM user manual): (a) To generate the tribofilm, the ball is loaded against the disk, and run with a preset load and slide-to-roll ratio.

The maximum normal load in the MTM is 75 N, which corresponds to a maximum (mean) compressive Hertzian stress of 1.2 (0.80) GPa for standard steel balls and discs. Based on prior work, increasing the stresses beyond this limit is crucial to promote tribofilm growth within reasonable time frames (3,4). We thus used tungsten carbide (WC) balls and discs whose higher elastic modulus permits increasing the maximum Hertzian stress to 2.6 GPa (4). Note that many studies report tribofilm growth on standard steel materials in the MTM. However, these studies were conducted under mixed or boundary lubrication conditions where the maximum stresses at individual asperity contacts are much higher than the idealized Hertzian stress expected in the fluid.

The test specimens and the material properties are shown in **Table S2**. The root-mean-square roughness of the ball and the disc was measured using a Zygo NewView™ 6300 (Middlefield, CT) white light interferometer. The measurement length is approximately 700 µm. A cut-off length of 80 µm was applied to minimize the curvature effect from the specimens (5). The values were averaged from six repeated measurements.

	WC ball	**WC disc**
Diameter	19.05 mm	46 mm
σ	5 nm	2 nm

WC material properties	
E	600 GPa
ν	0.293

Table S2. Test specimen information and material properties

Before each experiment, the specimens were sonicated in toluene and isopropanol for 15 minutes each, and dried using compressed nitrogen gas. A Kimwipe was gently wiped on the specimens to remove fibers or any other residues. After each experiment, all the MTM and SLIM components and test specimens were sonicated in toluene and isopropanol again for 15 mins. Droplets of 0.05M of ethylenediaminetetraacetic acid (EDTA) solution were applied to the film area of the test specimen for 1 minute to remove the ZDDP tribofilm (6). Then, a 15-min sonication with deionized (DI) water to remove EDTA residue. This procedure allowed for re-use of the WC specimens multiple times before visible signs of surface distress were noted.

2.2   ToF-SIMS experiment

The ToF-SIMS analysis was carried out with a xenon (Xe^+) primary ion source with 10kV energy and 10 nA of current, and with a spatial resolution of 256 x 256 pixels. A large 400 x 400 µm^2 field of view was used; this reduces the risk of unintentionally damaging the tribofilm. The method for collecting sample data is shown in **Figure S2 (a)**. To convert the unit of depth from number of frames to thickness in nm, an approximate calibration was made. The average height

of the tribofilm shown in **Figure S2(c)** was estimated to be 80 nm from the WLI measurement in **Figure S2(b)**. After ToF-SIMS measurement milling for 8000 frames, the trench was found to be approximately 200-nm deep shown in **Figure S2(e)** from the WLI measurement in **Figure S2(d)**. Therefore, the depth resolution of this study is around 0.035 nm/frame.
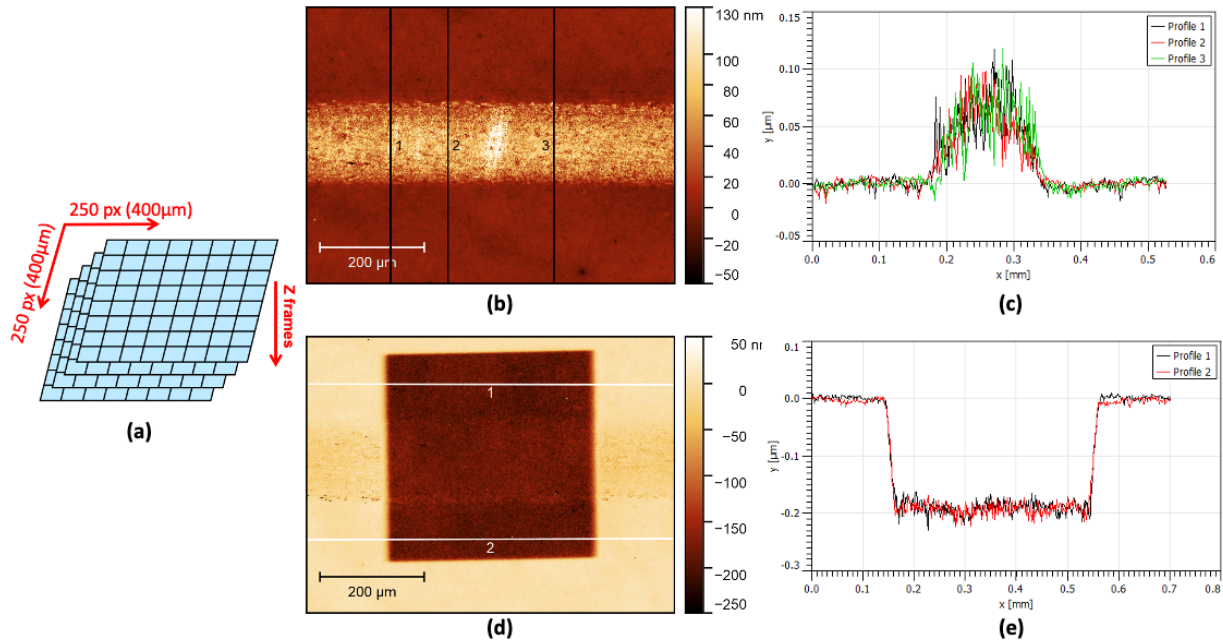

Figure S2. (a) Schematic illustration of the ToF-SIMS measurement in x, y, and z directions [adapted from Tescan manual]. (b) The WLI image of the running track on the WC disc before the ToF-SIMS experiment and (c) the corresponding average height of tribofilm, measured from 3 different line profiles. (d) The WLI image of the running track on the WC disc after 8000-frame of milling from ToF-SIMS experiment, and (e) the average height in the tribofilm area.

3. Characterizing test fluid properties

3.1 Traction Behavior

To measure the shear stress for each blend, the traction behavior of each fluid was characterized at applied loads varying between 23.5 to 68 N. This range yields Hertzian maximum contact stresses from 1.75 to 2.5 GPa as shown in **Table S3**. For each load condition, the test temperature was varied at 20°C intervals from 20°C to 140°C.

F (N)	P_{max} (GPa)	R (µm)
23.5	1.75	80
38	2	93.9
40	2.1	95.5
46.5	2.2	100.4
49.5	2.25	102.5
53	2.3	104.9
60.5	2.4	109.6

| 68 | 2.5 | 114 |

Table S3. Summary of applied load with the corresponding idealized Hertzian stress, and contact radius.

For the traction experiments, the entrainment speed was held at 2000 mm/s and the slide-to-roll Ratio (SSR), as defined in equation (S1), was varied from 0 to 100%:

$$SRR = \frac{|U_{disc} - U_{ball}|}{U} \text{ x } 100\% \qquad (S1)$$

PIB was selected due to its high traction coefficient in EHL conditions. **Figure S3(a)** compares the traction response between the PIB and the PAO. Since PIB exhibits higher EHL traction than PAO, it can generate a much greater traction coefficient at any SRR. By mixing these two fluids together, it is possible to create fluids with various of traction properties. This allows us to independently control the shear stress within the contact zone at any given normal stress and temperature.

The PIB traction curve in **Figure S3(b)** reaches a maximum at approximately 10% SRR. The reduction in traction at higher SRR is known as the thermal EHL region, when frictional heating of the lubricant in the inlet and contact region acts to lower the effective viscosity, and hence the shear stress (7). To reduce the effect of frictional heating, all of the MTM-SLIM film-forming experiments were performed at 6% SRR. The traction response of each blend at this SRR is below the maximum traction coefficient for each test fluid but is sufficiently high to generate a ZDDP tribofilm.
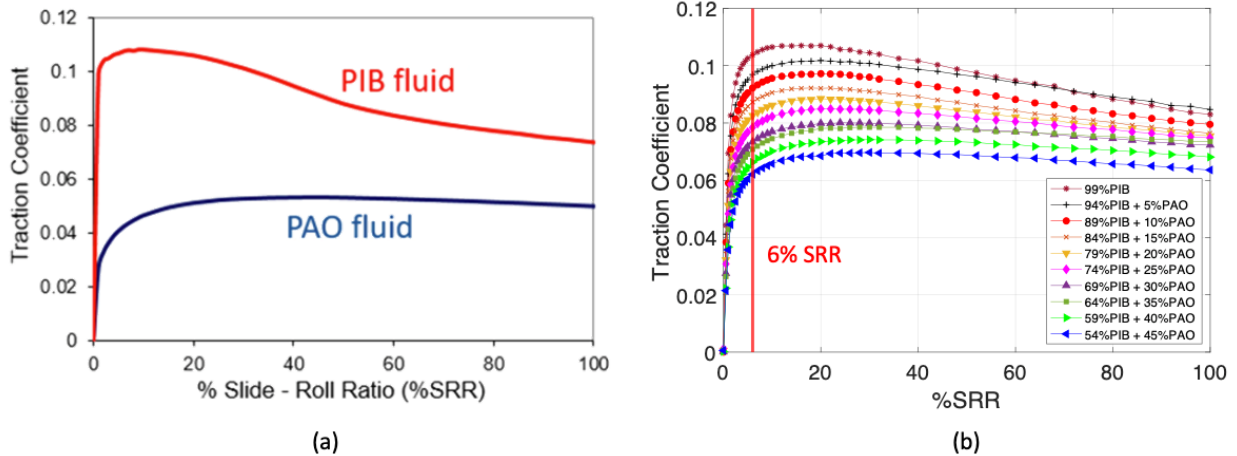

(a)

(b)

Figure S3. (a) The traction curves of PIB and PAO fluids under 2.5 GPa and 100°C. (b) EHL traction coefficient as a function of SSR for different blends at 2.5 GPa and 140°C. 6% SRR was used for all tribofilm experiments to eliminate frictional heating.

The shear stress is estimated by using the maximum Hertzian stress, and the measured traction coefficient:

$$\tau_{max} = \mu_{6\%SRR} P_{max} \qquad (S2)$$

A summary of maximum shear stresses generated at 6% SRR as a function of composition at different temperatures and compressive stress is shown in ***Figure S4***. Under different conditions, it was possible to vary the shear stress between 80 MPa to 264 MPa.
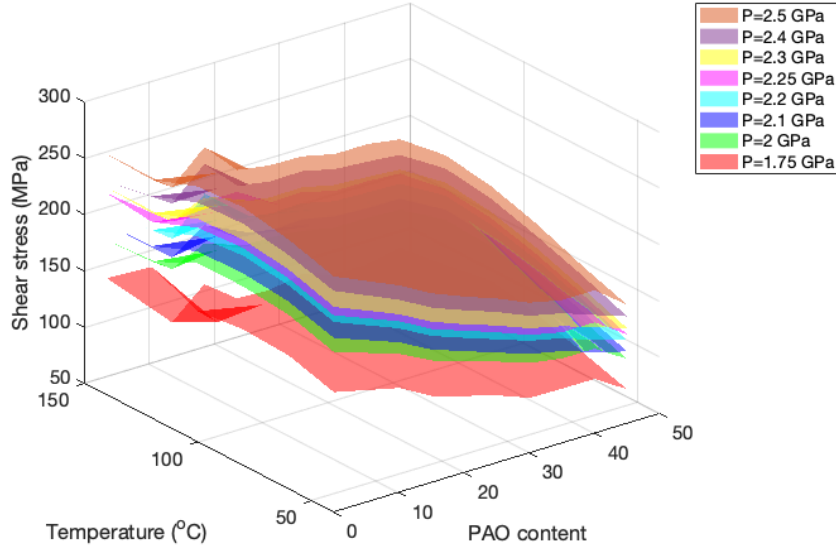

Figure S4. Maximum shear stress as a function of composition at different temperatures and pressures (6% SRR).

3.2 Specific film thickness characterization

To ensure there is no surface contact in our experiments, we used equation (S3) to calculate specific film thickness (8):

$$\lambda = \frac{h_c}{\sqrt{\sigma_{ball}^2 + \sigma_{disc}^2}} \tag{S3}$$

Typically, $\lambda > 3$ implies a full elastohydrodynamic condition in which there is no surface contact. The central film thickness, h_c, can be determined by using Cheng's equation (9) in equation (4) .

$$h_c = 1.415 R_a * \left(\frac{\eta_0 \alpha U}{R_a}\right)^{0.725} * \left(\frac{P}{E_a}\right)^{-0.174} \tag{S4}$$

Where U is the entrainment speed:

$$U = \frac{1}{2}(U_{ball} + U_{disc}) \tag{S5}$$

The central film thickness of different blends was measured using the PCS instruments optical EHL apparatus. An example of EHL film thickness measurement as a function of rolling

speed is shown in *Figure S5*. From these measurements, it is possible to extract the missing lubricant-related properties in equation (4). Using the calculated lubricant properties for each blend it is possible to reapply equation (4) to the materials and operating conditions in the MTM experiments. The resulting film thickness values are then used in equation (3) to calculate the specific film thickness. The specific film thickness of all experiments is greater than 15, which corresponds to the case of 54 wt% PIB + 45 wt% PAO blend at 140°C and 2.5 GPa. This shows that there is a high degree of separation between the surfaces.
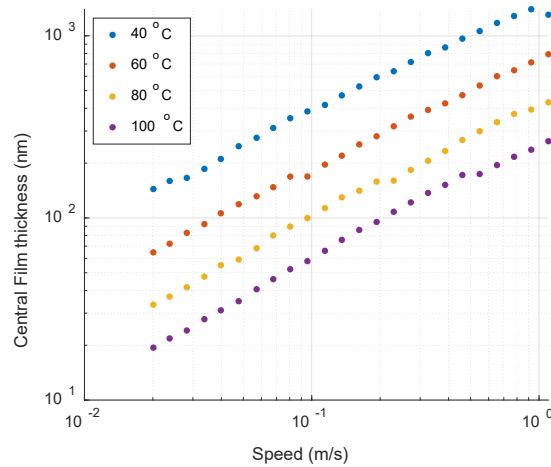

Figure S5. EHL film thickness of 64%PIB + 35% PAO in pure rolling.

3.3 Tribofilm thickness measurement

An example of a SLIM image is shown in *Figure S6*. The image resolution is 0.7 μm per pixel. The film thickness at each pixel is extracted using the combination of the refractive index of the lens and tribofilm as listed in *Table S4* and the measured values from the optical measurement (10).

	Refractive index	Reference
MTM lens	1.4	(2)
ZDDP tribofilm	1.6	(6)

Table S4. The refractive index of MTM lens and ZDDP tribofilm.

For our calculations of average tribofilm thickness we used a circular analysis area of 144 μm in diameter. This value corresponded to the largest width of the tribofilm that was produced. After obtaining a series of SLIM images during the test, the film thickness and volumetric growth over time can be calculated.
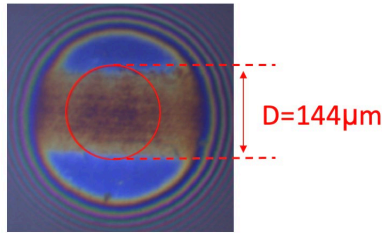
Figure S6. An example of a SLIM image of a ZDDP tribofilm.

3.4 Tribofilm Growth and Morphology

To capture the initial fast growth of the tribofilm, especially with high shear stress and temperature, the interference image was taken more frequently in the initial time interval. The frequency of different time intervals is summarized in **Table S5**.

Time	SLIM Imaging Frequency
0—10 minutes	Every 1 minute
10—30 minutes	Every 5 minutes
30—60 minutes	Every 10 minutes
60—360 minutes	Every 30 minutes

Table S5. The frequency of SLIM images taken at different time periods.

An example of a series of SLIM images obtained with 99%PIB + 1% ZDDP from a 360-minute test is shown in **Figure S7**. A patchy tribofilm was observed to grow initially in the middle of the contact, where both the normal and shear stress is at the maximum value. It appears that the growth extends from this region toward the edges. A possible explanation is that the Hertzian stress reduces away from the center of the contact and thus it takes longer for the film to grow in areas away from the central region. The corresponding traction coefficient in **Figure S8** shows that the shear stress stays almost constant during the experiment.
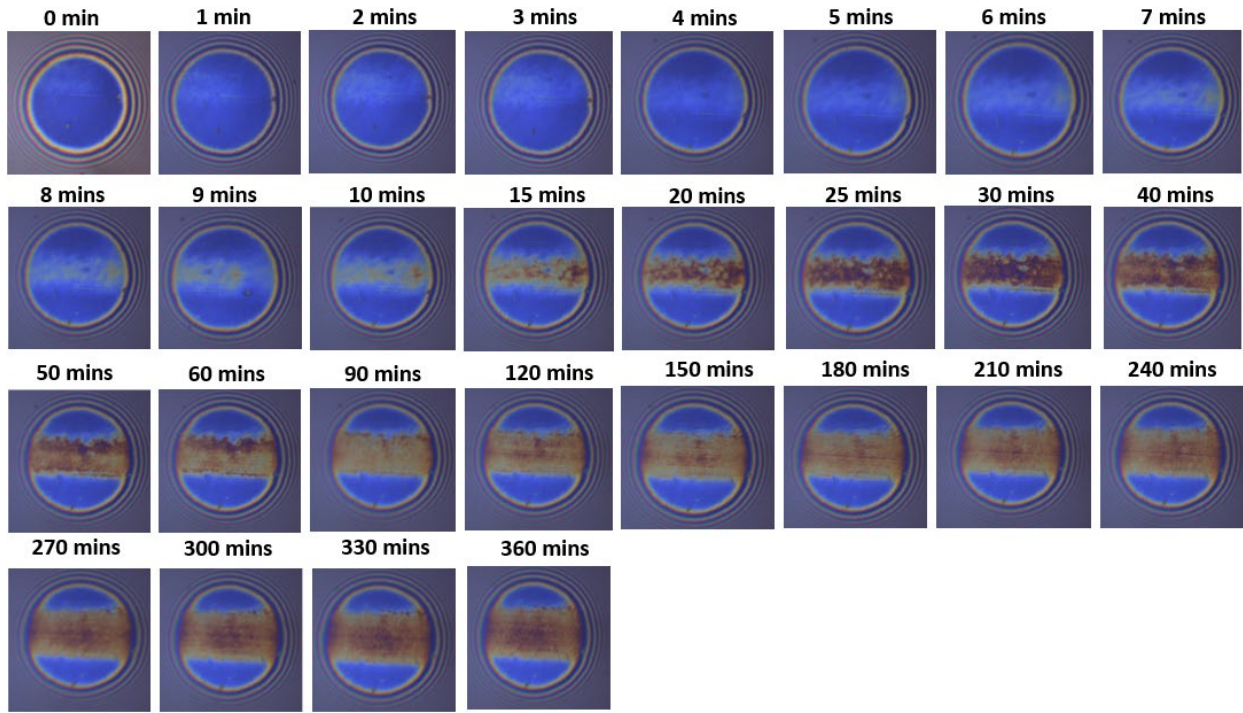
Figure S7. SLIM images of ZDDP tribofilm formation with 99%PIB + 1% ZDDP at 140°C under 2.5 GPa applied stress, which corresponds to 260 MPa shear stress.
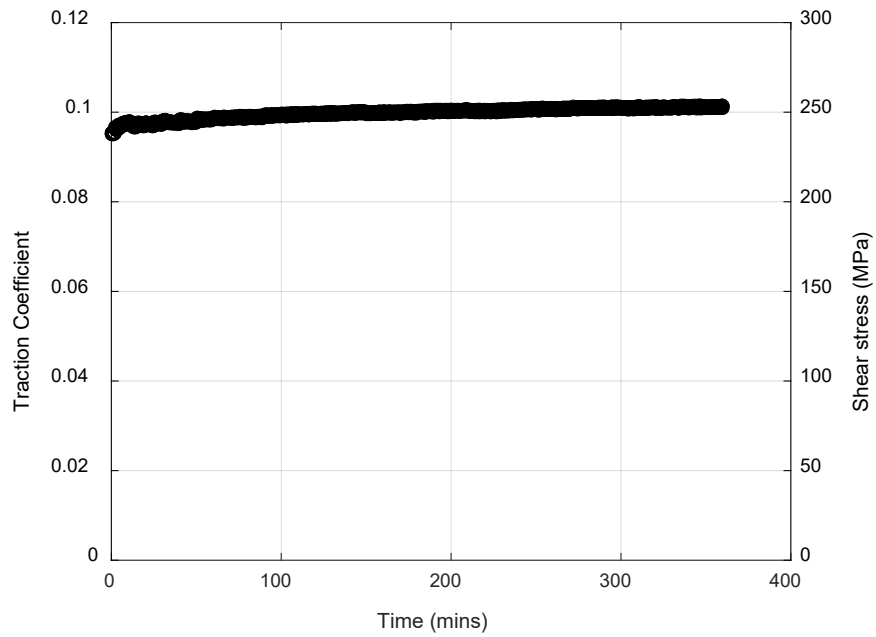

Figure S8. The traction coefficient (the shear stress) is stable over time with 99%PIB + 1% ZDDP under the compressive stress of 2.5 GPa at 140°C

Figure S9 shows the corresponding film growth dynamics based on averages calculated over the area shown in *Figure S7*. At this shear stress (260 MPa), the tribofilm thickness rapidly reached a maximum at 30 minutes, then started to decline before continuing to grow back to approximately the same thickness. A similar effect was observed by Gosvami *et al.* in AFM-based growth experiments which have high spatial resolution of the tribofilm, and was attributed to the competition between film growth and removal (3). In our case, since direct physical contact is unlikely to have occurred during the sliding experiment, this film removal and formation could indicate that there are some inherent properties of the ZDDP tribofilm that limit the growth mechanisms. Ueda *et al.* explored the crystalline structure of ZDDP tribofilms grown in MTM under boundary lubrication conditions, where the outer region of the tribofilm is amorphous and can be easily removed, while the inner region is nanocrystalline, which is thus assumed to be much stronger and durable (11). The removal of tribofilm observed here indicates that the weaker amorphous structure of the outermost region tribofilm could not withstand the shear-induced by the fluid. After this transient period where the amorphous region is presumably removed, the formation rate modestly exceeds the removal rate, since the nanocrystalline structure in the bottom of the tribofilm cannot be removed easily.
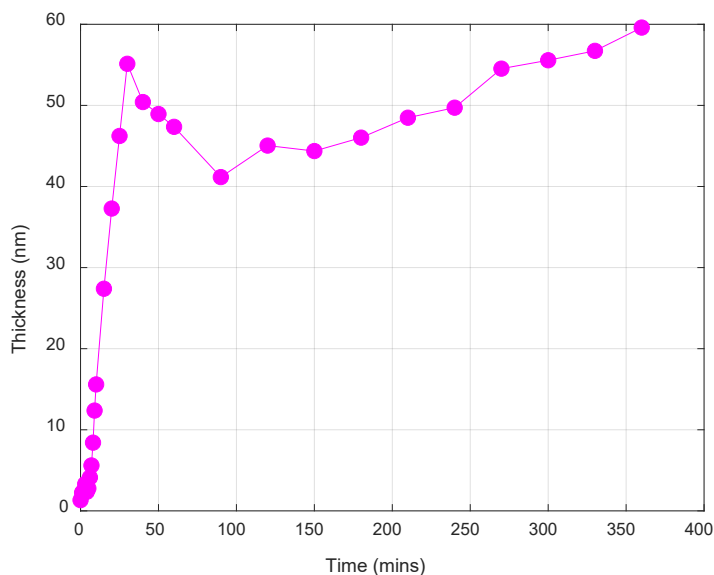

Figure S9. The evolution of the average thickness of a ZDDP tribofilm growth with 99%PIB + 1% ZDDP at 140°C under 2.5 GPa applied stress, which corresponds to 260 MPa shear stress.

In this study, we observed that the thickness reaches to a saturation at 30 minutes with higher traction fluid at higher shear stress and higher temperautre. On the other hand, there is a very thin film deposited for the first 10 minutes with lower traction fluid at low shear stress and low temperature, thus the thickness cannot be accurately measured by the SLIM system.

Therefore, the data between 10 to 30 minutes are included for the volumetric growth rate calculation, with a linear fit performed for all the experiments.

The tribofilm growth vs. time was recorded under different conditions. For the shear stress study, *Figure S10(a)* and *Figure S10(c)* show the variation of both tribofilm thickness and volume under the condition listed in experiment Subset 1 and Subset 2 respectively in *Table 2*. As specified above, the growth rates were extracted using a linear fit from 10 to 30 minutes as shown in *Figure S10(b)* and *Figure S10(d)*. Similarly, the tribofilm responses of the two experimental subsets of temperature and compressive stress are displayed in *Figure S11* and *Figure S12* respectively. The extended Eyring model fit is performed using the curve fitting function in Matlab. The error bar is the 95% confidence interval calculated by Matlab.
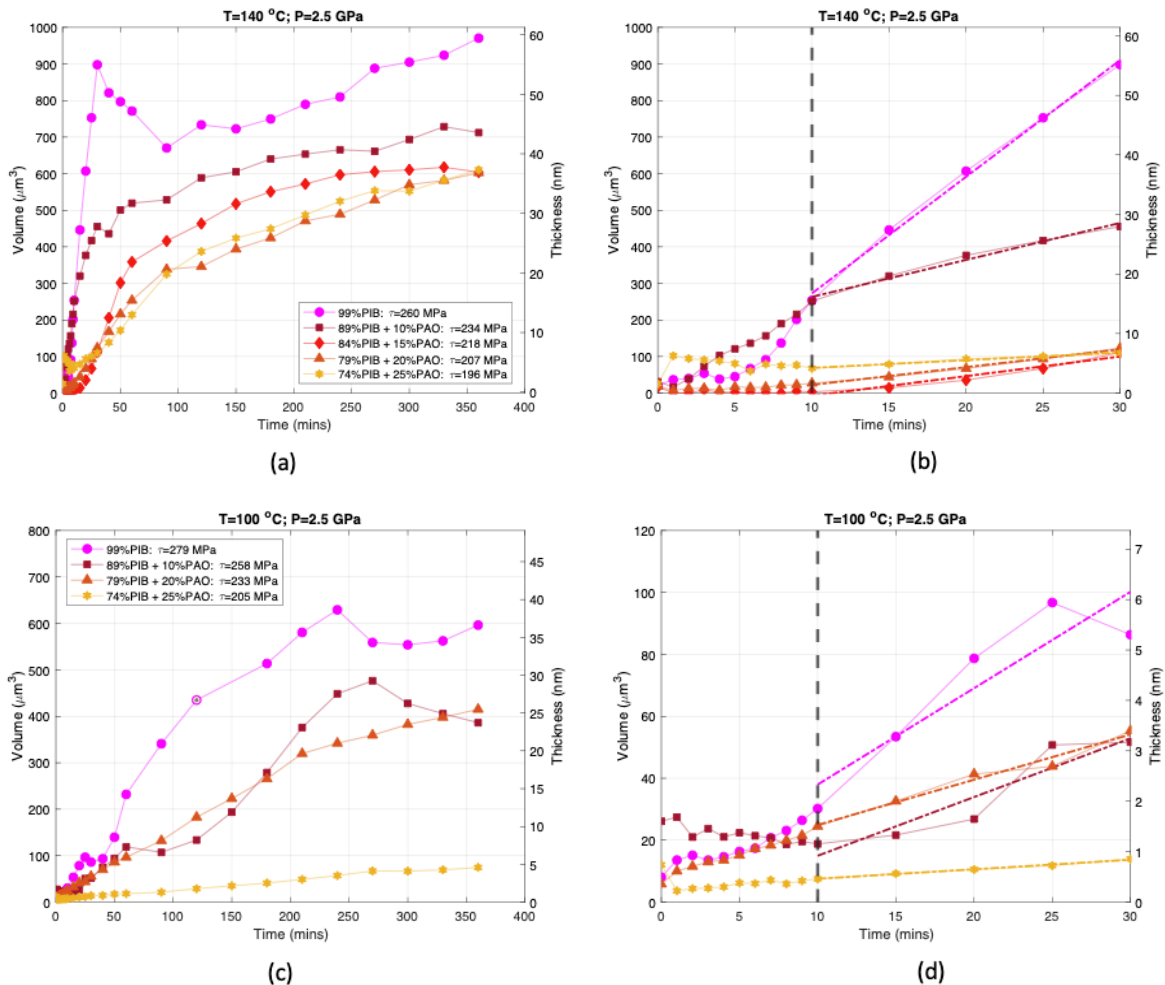

Figure S10. Effect of shear stress on tribofilm formation for (a) experiment Subset 1: T=140°C & P=2.5 GPa with the first 30 minutes shown in (b), and (c) experiment Subset 2: T=100°C; P=2.5 GPa with the first 30 minutes shown in (d). The growth rates were estimated from a linear fit between 10 to 30 minutes for experiment Subset 1 and experiment Subset 2 as shown in (b) and (d).
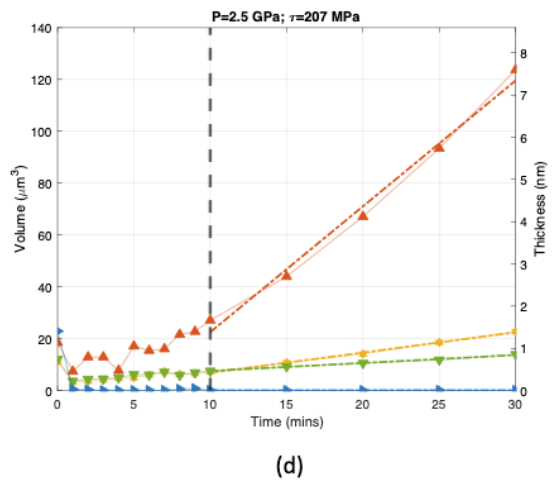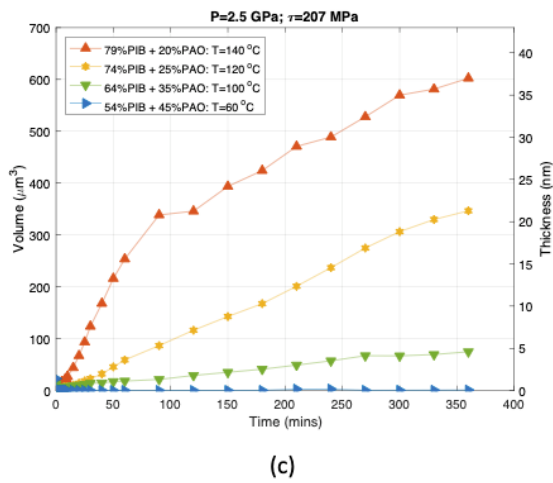
Figure S11. Effect of temperature on tribofilm formation of (a) experiment Subset 1: P=2.5 GPa; τ=233±2 MPa with the first 30 minutes shown in (b), and (c) experiment Subset 2: P=2.5 GPa; τ=207±2 MPa with the first 30 minutes shown in (d). The growth rates were estimated from a linear fit between 10 to 30 minutes for experiment Subset 1 and experiment Subset 2 as shown in (b) and (d).
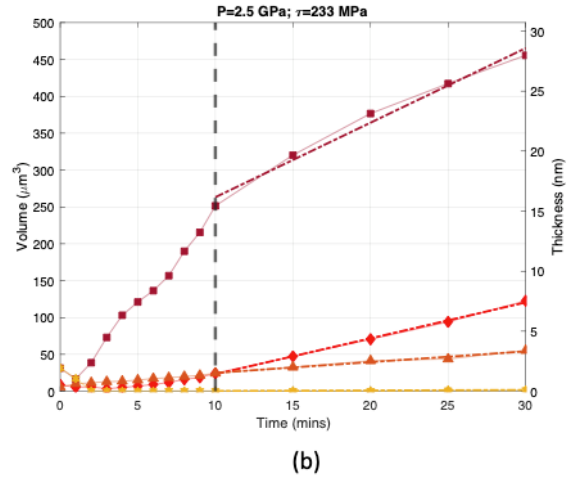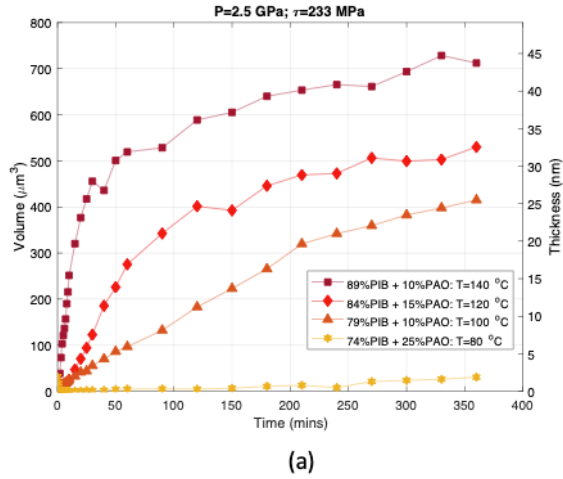
Figure S12. Effect of compressive stress on tribofilm formation of (a) experiment Subset 1: T=140°C; τ=194±2 MPa with the first 30 minutes shown in (b), and (c) experiment Subset 2: T=120°C; τ=207±2 MPa with the first 30 minutes shown in (d). The growth rates were estimated from a linear fit between 10 to 30 minutes for experiment Subset 1 and experiment Subset 2 as shown in (b) and (d).
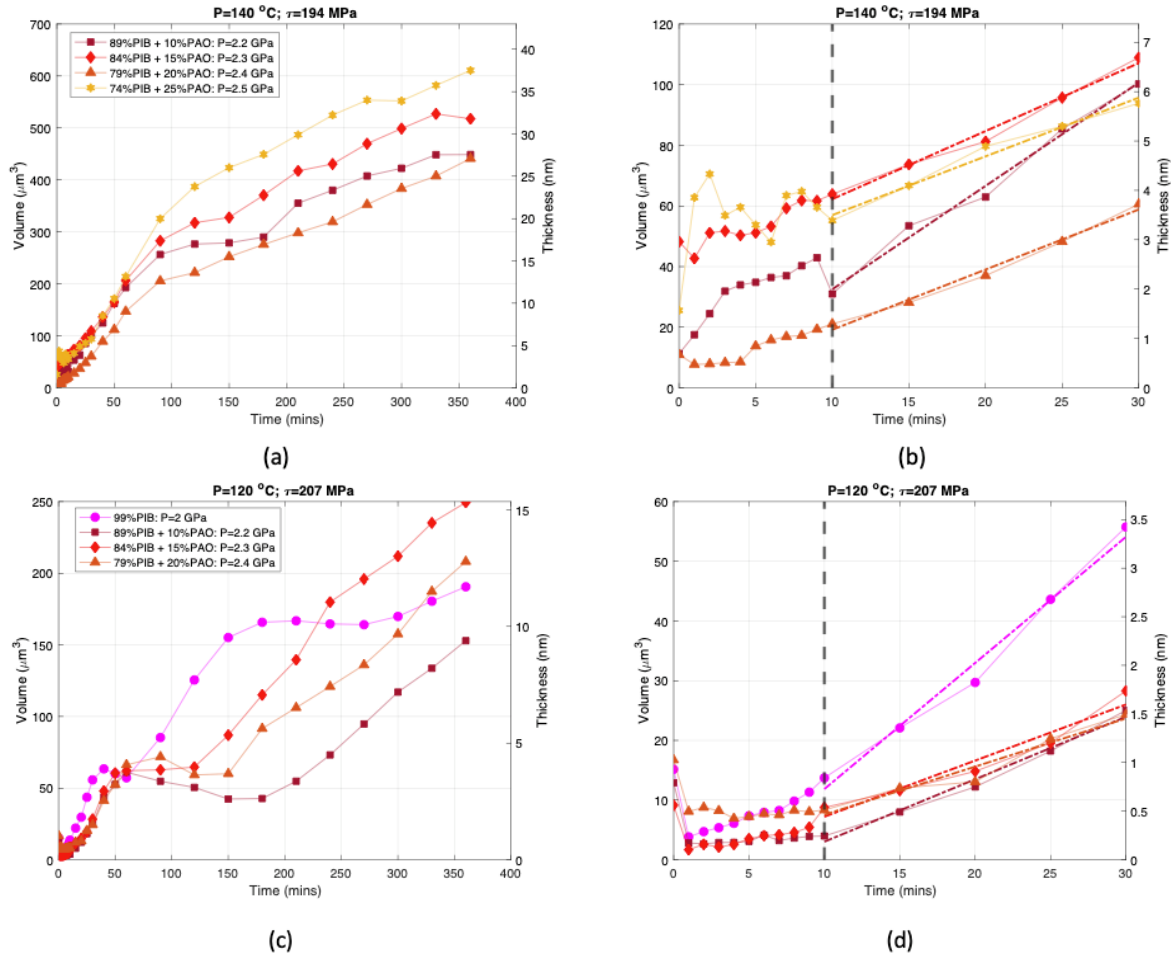
Note that this study uses the maximum compressive stress and maximum shear stress values for fitting the extended Eyring model to determine the activation energy and volume for each data set. Based on the Hertizan stress model, the mean stress is 2/3 of the maximum stress. If the mean compressive stress and shear stress were used in the extended Eyring model fit, and using $\Delta U_{act} = 0.54 \ eV$ from Table 4, $\Delta V_{act} = 0.27 \ nm^3$ and $\Delta \Omega_{act} = 0.0132 \ nm^3$ were obtained. Those values are approximately 3/2 of the values shown in Table 4 as expected. We note that some literature papers use the mean stress instead of the maximum stress and so care should be taken in comparing values between different publications. This lack of standardization is a concern, but we believe an even more significant issue is the fact that the stress values are in fact not constant throughout the contact. This will be addressed in a future publication.

Since the fluid viscosities of our oils are high, sometimes during the SLIM measurement the oil will get trapped at the center of the contact when the ball is initially put in contact with the SLIM window, particularly when the test temperature is low. *Figure S13* shows an example of oil trapped at the center of the contact. When analyzing the tribofilm thickness, we avoided the oil pocket area. Despite this, the oil pocket is sometimes too large in the beginning period of some of our tests, especially the first 10 mins, and it was not possible to avoid having the oil pocket be within the pre-defined SLIM analysis area for determining film thickness. Therefore, the oil pocket sometimes leads to a misleadingly high film thickness in early tribofilm thickness measurements. This can be seen, for example, in *Figure S10(d)* for the 89%PIB + 10% PAO data set. This artifact diminished after the initial 10 minutes due to the formation of tribofilm on the surface. One way to reduce the effect is to increase the hold time between the ball and the microscope when doing the SLIM imaging. This allows the trapped oil to leak away. However, that would add significant time to the experiment, and was not performed so that all the experiments could be conducted with the same timing
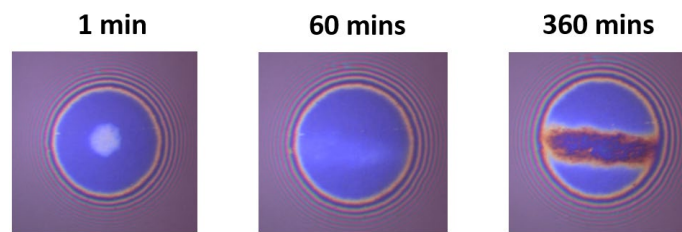

Figure S13. An example of oil trapped at the center of the contact for 89%PIB+10%PAO under 2.5 GPa at 100˚C

4. Nomenclature

E	Young's modulus
E_a	Reduced Young's modulus
F	Applied load
h_c	EHL central film thickness
P_{max}	Maximum Hertzian pressure
R	Contact radius
R_a	Reduced radius
SRR	Slide-to-roll ratio
U	Entrainment speed
U_{ball}	MTM ball speed
U_{disc}	MTM disc speed

α	Pressure-viscosity coefficient
η	Dynamic viscosity
η_0	Dynamic viscosity at atmospheric pressure
λ	Specific film thickness
μ	Traction coefficient
ν	Poisson's ratio
σ	RMS roughness
τ_{max}	Maximum shear stress

5. Reference

1. D02 Committee. Test Method for Density, Relative Density, and API Gravity of Liquids by Digital Density Meter [Internet]. ASTM International; [cited 2021 Jul 26]. Available from: http://www.astm.org/cgi-bin/resolver.cgi?D4052-18A

2. Spikes HA, Cann PM. The development and application of the spacer layer imaging method for measuring lubricant film thickness. Proc Inst Mech Eng Part J J Eng Tribol. 2001 Mar 1;215(3):261–77.

3. Gosvami NN, Bares JA, Mangolini F, Konicek AR, Yablon DG, Carpick RW. Mechanisms of antiwear tribofilm growth revealed in situ by single-asperity sliding contacts. Science. 2015 Apr 3;348(6230):102–6.

4. Zhang J, Spikes H. On the Mechanism of ZDDP Antiwear Film Formation. Tribol Lett. 2016 Aug;63(2):24.

5. Kadiric A, Sayles RS, Zhou XB, Ioannides E. A Numerical Study of the Contact Mechanics and Sub-Surface Stress Effects Experienced Over a Range of Machined Surface Coatings in Rough Surface Contacts. J Tribol. 2003 Oct 1;125(4):720–30.

6. Dawczyk J, Morgan N, Russo J, Spikes H. Film Thickness and Friction of ZDDP Tribofilms. Tribol Lett. 2019 Jun;67(2):34.

7. Lafountain AR, Johnston GJ, Spikes HA. The Elastohydrodynamic Traction of Synthetic Base Oil Blends. Tribol Trans. 2001 Jan;44(4):648–56.

8. Stachowiak GW, Batchelor AW. Elastohydrodynamic Lubrication. In: Engineering Tribology. Elsevier; 2014. p. 293–370.

9. Cheng HS. A numerical solution of the elastohydrodynamic film thickness in an elliptical contact. J Tribol Technol. 1970 Jan 1;92(1):155–61.

10. Fujita H, Spikes HA. The formation of zinc dithiophosphate antiwear films. Proc Inst Mech Eng Part J J Eng Tribol. 2004 Apr;218(4):265–78.

11. Ueda M, Kadiric A, Spikes H. On the Crystallinity and Durability of ZDDP Tribofilm. Tribol Lett. 2019 Dec;67(4):123.